Supplementary Material

All-element recovery and regeneration of mixed $LiNi_xCo_yMn_{1-x-y}O_2/LiFePO_4$ cathode materials by synergistic redox processes

Jingtian Zou[1], Dezhao Peng[1], Wenyang Hu[1], Shilin Su[1], Xiaowei Wang[1*], Zaowen Zhao[2*], Shubin Wang[3], Di He[4], Pengfei Li[5], Jiafeng Zhang[1*]

1 National Engineering Laboratory for High-Efficiency Recovery of Refractory Nonferrous Metals, School of Metallurgy and Environment, Central South University, Changsha 410083, PR China
2 Special Glass Key Lab of Hainan Province, School of Materials Science and Engineering, Hainan University, Haikou 570228, China
3 State Environmental Protection Key Laboratory of Environmental Pollution Health Risk Assessment, South China Institute of Environmental Sciences, Ministry of Ecology and Environment (MEE), Guangzhou, 510655, China
4 Key Laboratory for City Cluster Environmental Safety and Green Development of the Ministry of Education, School of Ecology, Environment and Resources, Guangdong University of Technology, Guangzhou, 510006, PR China
5 Anhui Winking New Material Technology Co., LTD, Fuyang 236000, PR China

Supporting information: 8 tables, 15 figures

Experimental section

Materials and reagents

Spent $LiFePO_4$ (S-LFP) and spent $LiNi_xCo_yMn_{1-x-y}O_2$ (S-NCM) electrodes attached to current collector aluminum foil were obtained from Zhejiang Huayou Cobalt Co., Ltd (Zhejiang, China). All the chemical reagents used were reagent grade, including sulfuric acid (H_2SO_4, AR, 98.3%), sodium carbonate (Na_2CO_3, AR, 99.5%), and glucose ($C_6H_6O_6$, AR, 99.5%), were purchased from Macklin Co. Ltd.), and all stock solutions were prepared with deionized (DI) water. The main chemical components of S-LFP and S-NCM are shown in Table S1 and Table S2. Figure S4 shows the XRD pattern of spent LFP cathode materials. The XRD pattern of spent NCM cathode materials and magnification of (101) and (104) peaks was shown in Figure S5.

Table S1 The main element content of S-LFP cathode electrodes

Element	Fe	Al	Li	P	C	Cu
Content (wt%)	30.6	0.84	3.85	16.9	6.52	0

Table S2 The main element content of S-NCM cathode electrodes

Element	Li	Ni	Co	Mn	C	Cu	Al	Fe
Content (wt%)	3.56	11.99	9.16	18.08	38.42	1.7	1.27	0.56

Experimental Methods

The spent mixed NCM/LFP were pretreated by discharge, disassembly, and separation. The positive active material is picked out and mixed with 100 ml of sulfuric acid in a 500 ml glass reactor in proportion, and the glass reactor was heated in a magnetic stirrer (Shanghai, DF-101S), and a magnetic rotor stirred the solution. A temperature controller probe was also inserted to observe the temperature of the leaching reaction in real-time. After the reaction, the solution is pumped and filtered,

where the filtrate goes through a series of treatments to obtain Li_2CO_3 and precursors of NCM cathode materials, the filtrate residue is used in the regeneration of LFP after separation and purification.

The leaching rate of Li, Ni, Co, and Mn was calculated by equations (S1):

$$R = \frac{C_1 \times V_1}{m_0} \times 100\% \quad (S1)$$

Where R is the leaching rate of Li, Ni, Co and Mn, %; m_0 is the initial Li, Ni, Co, and Mn concentrations in spent mixed NCM/LFP, mg; C_1 is the Li, Ni, Co, and Mn concentrations in leachate after treatment, mg/L; V_1 is the volume of leachate, L.

NCM precursor was obtained by coprecipitation after removing copper, iron, and aluminum from leachate, mixed with Li_2CO_3 and glucose, and sintered to obtain the regenerated NCM. Roasting conditions were raising the temperature to 500 ^oC and holding for 10 hours, then raising the temperature to 800 ^oC and holding for 16 hours, and cooling to room temperature for 4 hours. The recovered FPO powder was collected as a precursor, mixed with Li_2CO_3 and glucose, and sintered to obtain the regenerated LFP. Roasting conditions were raising the temperature to 750 ^oC for 4 h and holding for 10 hours, then cooling to room temperature for 4 hours.

Characterization

After the leachate was diluted to a concentration that could be detected, its elemental content was analyzed by an inductively coupled plasma emission spectrometer (ICAP7400, Thermo, USA). The X-ray diffraction analysis of the raw material and leachate was performed by an X-ray diffractometer (TTR III, Rigaku, Japan) equipped with a copper target at a power of 18 kW. The analysis and comparison of the diffraction patterns were carried out with the help of JADE software. The morphology and structure of the leached residue were studied by field emission scanning electron microscopy. The elemental distribution was illustrated with an energy dispersive spectrometer (SEM-EDS) (XL30 ESEM-TMP Philips-FEI, The Netherlands) at an accelerating voltage of 10-20 kV, and energy spectroscopy was performed. The valence state of the elements was characterized by X-ray

photoelectron spectroscopy (XPS, Thermo Fisher Scientific K-Alpha, China).

Text 1

Thermomechanical analysis

The possible reactions:

$$LiFePO_4 + H^+ + \frac{1}{4}O_2 = Li^+ + Fe^{3+} + PO_4^{3-} + \frac{1}{2}H_2O \quad (S2)$$

$$LiFePO_4 + Fe^{3+} = FePO_4 + Li^+ + Fe^{2+} \quad (S3)$$

$$LiNi_xCo_yMn_{1-x-y}O_2 + Fe^{2+} + 4H^+ = Li^+ + xNi^{2+} + yCo^{2+} + (1-x-y)Mn^{2+} + Fe^{3+} + 2H_2O \quad (S4)$$

$$LiCoO_2 + Fe^{2+} + 4H^+ = Li^+ + Co^{2+} + Fe^{3+} + 2H_2O \quad (S5)$$

$$Co_3O_4 + 2Fe^{2+} + 8H^+ = 3Co^{2+} + 2Fe^{3+} + 4H_2O \quad (S6)$$

$$MnO_2 + 2Fe^{2+} + 4H^+ = Mn^{2+} + 2Fe^{3+} + 2H_2O \quad (S7)$$

$$CoO + 2H^+ = Co^{2+} + H_2O \quad (S8)$$

$$MnO + 2H^+ = Mn^{2+} + H_2O \quad (S9)$$

$$NiO + 2H^+ = Ni^{2+} + H_2O \quad (S10)$$

Table S3 The relevant thermodynamic data of target elements and sources:

Compound	Δ_rG^θ (KJ mol^{-1})	Resource
H^+	0	HSC 9.0
O_2	201.15	HSC 9.0
H_2O	-237.25	HSC 9.0
$LiFePO_4$	-1480.75	Reference
$FePO_4$	-1182.75	HSC 9.0
Li^+	-293.03	HSC 9.0
Fe^{3+}	-4.61	Reference
PO_4^{3-}	-1025.94	HSC 9.0
Fe^{2+}	-78.87	Reference
$LiNi_xCo_yMn_{1-x-y}O_2$	-	-
Ni^{2+}	-45.71	HSC 9.0
Co^{2+}	-54.50	HSC 9.0
Mn^{2+}	-228.10	HSC 9.0
$LiCoO_2$	-693.75	HSC 9.0

Co_3O_4	-923.05	HSC 9.0
CoO	-214.29	HSC 9.0
NiO	-211.68	HSC 9.0
MnO_2	-467.35	HSC 9.0
MnO	-363.00	HSC 9.0

The caculated equation of ΔG-pH:

$$mA + nH^+ = pB + qC \tag{S11}$$

$$\Delta_r G_T = \Delta_r G_T^\theta + RTInQ \tag{S12}$$

$$\Delta_r G_T = \Delta_r G_T^\theta + RTIn\frac{[B]^p[C]^q}{[A]^m[H]^n} \tag{S13}$$

$$\Delta_r G_T = \Delta_r G_T^\theta + RTIn\frac{[B]^p[C]^q}{[A]^m} + 2.303nRTpH \tag{S14}$$

The caculated equation of ΔG-α:

$$mA + nB = pC + qD \tag{S15}$$

$$\Delta_r G_T = \Delta_r G_T^\theta + RTInQ \tag{S16}$$

$$\Delta_r G_T = \Delta_r G_T^\theta + RTIn\frac{[C]^p[D]^q}{[A]^m[B]^n} \tag{S17}$$

Table S4 The relevant equilibrium reactions of target elements and sources:

Equilibrium reactions	Ksp	Equations	Eq. no.
$NiSO_4(s)=Ni^{2+}+SO_4^{2-}$	2.9	$2.9 = [Ni^{2+}][\ SO_4^{2-}]$	(17)
$Ni(OH)_2(s)=Ni^{2+}+2OH^-$	2.0×10^{-15}	$2.0\times10^{-15}= [Ni^{2+}][\ OH^-]^2$	(18)
$Ni_3(PO_4)_2(s)=3Ni^{2+}+2PO_4^{3-}$	5.0×10^{-31}	$5.0\times10^{-31}= [Ni^{2+}]^3[\ PO_4^{3-}]^2$	(19)
$CoSO_4(s)=Co^{2+}+SO_4^{2-}$	5.4	$5.4= [Co^{2+}][\ SO_4^{2-}]$	(20)
$Co(OH)_2(s)=Co^{2+}+2OH^-$	1.6×10^{-15}	$1.6\times10^{-15}= [Co^{2+}][\ OH^-]^2$	(21)
$Co_3(PO_4)_2(s)=3Co^{2+}+2PO_4^{3-}$	2.0×10^{-35}	$2.0\times10^{-35}= [Co^{2+}]^3[\ PO_4^{3-}]^2$	(22)
$MnSO_4(s)=Mn^{2+}+SO_4^{2-}$	17.4	$17.4= [Mn^{2+}][\ SO_4^{2-}]$	(23)
$Mn(OH)_2(s)=Mn^{2+}+2OH^-$	1.9×10^{-13}	$1.9\times10^{-13}= [Mn^{2+}][\ OH^-]^2$	(24)
$Mn_3(PO_4)_2(s)=3Mn^{2+}+2PO_4^{3-}$	1.6×10^{-32}	$1.6\times10^{-32}= [Mn^{2+}]^3[\ PO_4^{3-}]^2$	(25)
$Li_2SO_4(s)=2Li^{+}+SO_4^{2-}$	126.8	$126.8= [Li^{+}]^2[\ SO_4^{2-}]$	(26)

$LiOH(s)=Li^{+}+OH^{-}$	28.4	$28.4=[Li^{+}][OH^{-}]$	(27)
$Li_3PO_4(s)=3Li^{+}+PO_4^{3-}$	3.2×10^{-9}	$3.2\times10^{-9}=[Li^{+}]^3[PO_4^{3-}]$	(28)

$$LiFePO_4+Fe^{3+}=Li^{+}+FePO_4+Fe^{2+} \qquad \Delta G^{\theta}=-66.461\ KJ/mol \tag{S18}$$

$$LiFePO_4+H^{+}+1/4O_2=Li^{+}+FePO_4+1/2H_2O \qquad \Delta G^{\theta}=-58.54\ KJ/mol \tag{S19}$$

Text 2:

Optimization of leaching conditions

The leaching rates of elements were studied at different temperatures, and it was found that temperature had little influence on the leaching rate. Therefore, the optimal leaching temperature was room temperature. The effect of H^+ concentration on the leaching efficiency was also studied, and it was found that the leaching efficiency increased with the increase of H^+ concentration, but stabilized at a high level close to 100% when the H^+ concentration was 1 mol L^{-1}. The effect of the solid-liquid ratio was also studied, and it was found that a solid-liquid ratio of less than 50 g L^{-1} was optimal for achieving a high leaching efficiency. Finally, the effect of reaction time was studied, and it was found that the leaching efficiency of Li, Ni, Co, and Mn increased with time and reached equilibrium after 40 min, with the leaching rate close to 100%. Therefore, the optimal reaction time was determined to be 40 min. Overall, optimizing the experimental parameters can greatly enhance the leaching efficiency of elements in the synergistic redox system, making it a promising approach for recycling spent mixed LFP/NCM. Figure S7 shows the leaching rates of Fe, P, Al and Cu under different conditions.

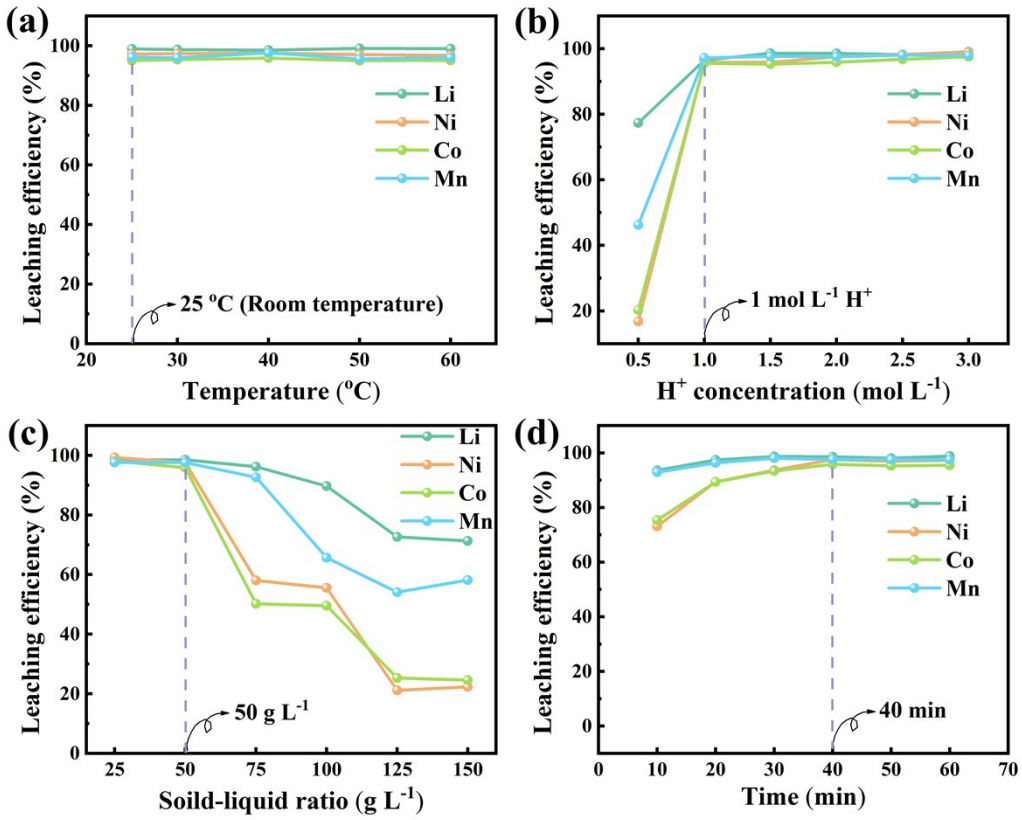

Figure S1. The effects on leaching efficiency for Li, Ni, Co, and Mn of (a) reaction temperature at 1 mol L^{-1} H^+ solution, S-L ratio of 50 g L^{-1} and 40 min; (b) H^+ concentration at 25 °C, S-L ratio of 50 g L^{-1} and 40 min; (c) solid-liquid ratio at 25 °C, 1 mol L^{-1} H^+ solution, and 40 min; (d) leaching time at 30 min, 25 °C, 1 mol L^{-1} H^+ solution and S-L ratio of 50 g L^{-1}.

Text 3

The mechanism researches

The dissolution of mixed LFP/NCM materials in the leaching process includes the following steps: (1) the reactants pass through the boundary layer; (2) the reactants transfer through the residue layer to the reaction interface; (3) chemical reaction at the particle interface; (4) the products diffuse through the residue layer and (5) the products transfer through the boundary layer to the fluid phase[14, 15]. According to the unreacted shrinking core model, the following three equations are represented as follows:

$$x = kt \tag{S20}$$

$$1 - \frac{2}{3}x - (1 - x)^{2/3} = kt \quad \text{(S21)}$$

$$1 - (1 - x)^{1/3} = kt \quad \text{(S22)}$$

where x represents the leaching efficiency and k is the rate constant of the reaction, and t is the reaction time.

To validate the control model of the reaction, each element was fitted and analyzed through the above model. Figure S10 shows the Data fitting diagram of internal diffusion at different temperatures and times for Li, Ni, Co, and Mn. The detailed kinetics parameters in Table S1-6 demonstrate that the external-diffusion-controlled model is unmatched due to the poor corresponding correlation coefficients (R^2). By contrast, the relatively higher R^2 value shows that the chemical-reaction controlled model is in good accordance with the kinetics data.

Furthermore, the apparent activation energy was also calculated via the Arrhenius equation:

$$k = Ae^{-\frac{E_a}{RT}} \quad \text{(S23)}$$

Where k is the reaction rate constant (min^{-1}) obtained from the kinetics plots; A is the pre-exponential factor; R is the universal gas constant (8.314 J K^{-1} mol^{-1}), and T is the absolute temperature (K). To simplify the calculation, the equation can be transformed into:

$$lnk = lnA - \frac{E_a}{RT} \quad \text{(S24)}$$

Text 4

Characterization of regenerated cathode materials

The XRD patterns of the regenerated material shown in Figure S2a are consistent with the standard pattern of NCM (#89-3601). O 1s characteristic peaks were detected in both S-NCM and R-NCM, as shown in Figure S2b. Deconvolution of the XPS spectrum of O 1s revealed the presence of distinct peaks of -C-O-, -C=O-, Li_2O, and -M-O-.[20]. The -C-O- and -C=O- peaks are associated with alkyl lithium carbonate ($ROCO_2Li$), ROLi, and Li_2CO_3, which are solvents used for decomposing carbonate electrolytes. The smaller amount of -C-O- and -C=O- bonds in R-NCM compared to S-NCM

indicates that there is less residue of organic matter, such as electrolyte, on the surface of R-NCM. The absence of organic matter on the surface of R-NCM, instead replaced by -M-O- and Li-O, suggests that the lithium deficiency and oxidation of the material were repaired after regeneration.[21]. The Ni 2p spectrum of S-NCM in Figure S2c involves two characteristic peaks at 874.5 eV and 855.8 eV for the Ni 2p1/2 and Ni 2p3/2 states, respectively[22]. The proportion of Ni distinct peaks in S-NCM is higher than that in R-NCM, indicating the reduction of the mixing of Li^+ and Ni^+, which helps maintain the cycle stability of the material after regeneration. [23, 24].The microstructure and composition of R-NCM in Figure S2d-o show uniformly dispersed particles with consistent size and secondary particle size similar to commercial materials. The HRTEM image reveals a lattice fringe with a d-spacing of 4.73 Å corresponding to the (003) plane of the rhomboidal $LiNiO_2$. The EDS element mapping images confirm the homogeneous distribution of Ni, Co, Mn, and O elements throughout the R-NCM electrode, confirming the formation of surface $LiNi_xCo_yMn_zO_2$[25].

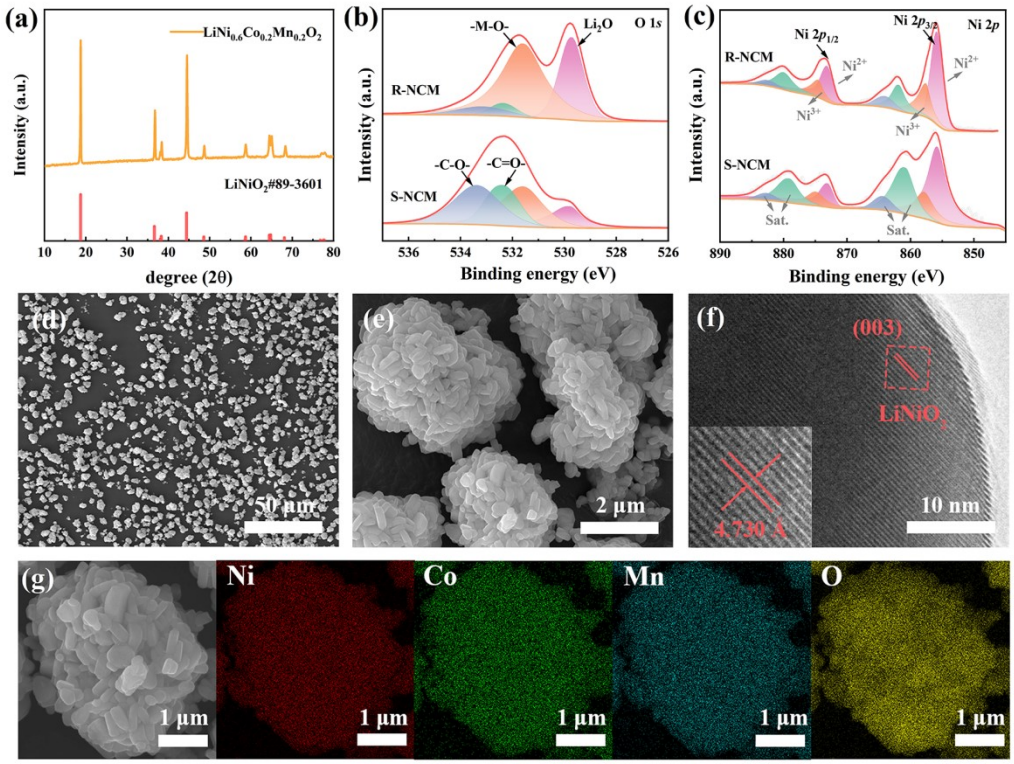

Figure S2. (a) XRD pattern of R-NCM; XPS spectra of (b) O 1s, (c) Ni 2*p*; SEM images of R-NCM at (d) 50 um and (e) 2 um scales; (f) HRTEM images of R-NCM particles; (g) Corresponding element mapping images of the R-NCM.

Electrochemical performance of regenerated NCM materials

To investigate the electrochemical properties of regenerated $LiNi_{0.6}Co_{0.2}Mn_{0.2}O_2$ cathode materials (R-NCM), the electrochemical tests were conducted in 2032-coin cells using lithium metal as the counter electrode. As shown in Figure S3a, the CV tests were processed at 2.7-4.3 V (vs. Li/Li^+) with a sweep speed of 0.1 mV s^{-1}. The redox peaks of R-NCM are observed 3.69/3.77 V for the second cycle, corresponding to the Ni^{2+}/Ni^{4+} redox reaction[12]. Figure S3b displays the charge/discharge curves at 1 C of R-NCM obtained by roasting at 800 °C. An initial discharge-specific capacity of 168.8 mAh g^{-1} is delivered for R-NCM, and the charge/discharge voltage performances range from 3.6-4.0 V, consistent with the CV results. The R-NCM shows a discharge capacity of 129.6 mAh g^{-1} after 300 charge and discharge processes and a capacity decay rate of 0.077% per cycle. The low capacity decay rate and constant voltage platform indicate that the R-NCM has excellent cycle stability. To evaluate the rate performance at different currents of R-NCM, the rate capacities are measured at 0.1 C, 0.2 C, 0.5 C, 1 C, 2 C, and 5 C (Figure S3 c and d), which reveal the discharge capacities of 183.4 mAh g^{-1}, 175.6 mAh g^{-1}, 163.8 mAh g^{-1}, 151.3 mAh g^{-1}, 137.1 mAh g^{-1} and 112.2 mAh g^{-1}, respectively. The discharge capacity increases to 144.3 mAh g^{-1} when the applied current is restored to 0.1 C, manifesting the good structure stability of R-NCM at a large current. Figures S12 and S13 show the XRD of the precursor to regenerated NCM and regenerated LFP.

The EIS test was carried out to analyze the lithium-ion diffusion kinetics differences between R-NCM and S-NCM. In Figure S3e, the Nyquist plots are composed of semicircles in the high-frequency zone and a slope line in the low-frequency region. The semicircle represents the charge-transfer resistance (Rct), and the slope line can be attributed to the lithium-ion diffusion rate. A noticeable drop in Rct from the R-NCM sample (21.3 Ω $rad^{1/2}$ $s^{-1/2}$) to S-NCM (106.8 Ω $rad^{1/2}$ $s^{-1/2}$) can be observed, proving the better electrochemical reaction kinetics performance of R-NCM material, which indicates that the regeneration process indeed improves the electrochemical performance of the cathode materials. Meanwhile, Figure S3f reveals the variation in lithium-ion diffusion kinetics by comparing

the different slope values. According to the lithium-ion diffusion coefficients regulation, the lithium-ion diffusion coefficients of R-NCM and S-NCM are calculated at 45.3×10^{-12} cm^2 s^{-1} and 1.79×10^{-12} cm^2 s^{-1}, respectively. It indicates that the recycled material has excellent lithium-ion diffusion speed.

$$D = \frac{R^2T^2}{2A^2n^4F^4C^2\sigma^2} \tag{S25}$$

D: lithium-ion diffusion coefficient; R: gas constant; T: temperature; A: electrode surface area; n: electron transfer number; F: Faradaic's constant, C: concentration of NCM material; σ: the slope of $z' \sim \omega^{-1/2}$.

To explore the cycle performance of recycled R-NCM materials, the electrochemical cycle stability of materials obtained from different roasting temperatures (750 °C, 800 °C, 850 °C) are compared, as shown in Figure S3g. The highest discharge capacity is realized in R-NCM roasted at 800 °C in the whole 300 charge/discharge cycles, which the electrochemical capacity of 148.9 mAh g^{-1}, 168.8 mAh g^{-1}, and 159.3 mAh g^{-1} in the first cycle at 1C for R-NCM roasted at 750 °C, 800 °C, and 850 °C, respectively.

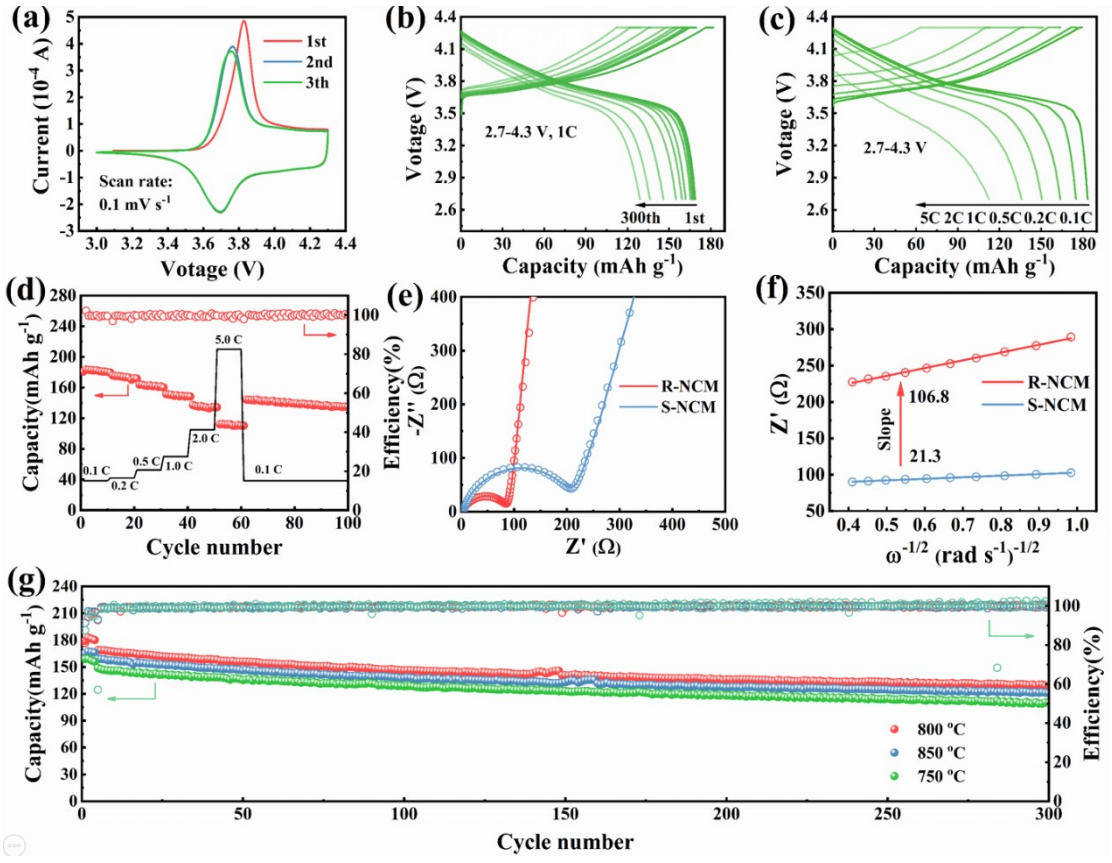

Figure S3. (a) CV curves of regenerated NCM obtained from the applied current of -1 mA, (b) charge/discharge profiles at 1 C from 1st to 300th cycles, (c) charge/discharge profiles at 0.1 C, 0.2 C,0.5 C,1 C,2 C and 5C, (d) the rate capability of R-NCM, (e) Nyquist plots in the frequency range of 0.01 Hz–100 kHz for S-NCM and R-NCM, (f) $z' \sim \omega^{-1/2}$ fitting curves of R-NCM and S-NCM obtained from the applied current of -1 mA, (g) the long cycling performance of R-NCM and S-NCM at 1 C .

The XRD pattern of reprepared $LiFePO_4$ materials have been shown in Figure S14.The recovered FPO and Li_2CO_3 were reconverted into $LiFePO_4$ (R-LFP). The surface chemical states of Li, Fe, P, and O in S-LFP, FPO, and R-LFP were investigated with XPS analyses. As shown by the survey spectra in **Figure S15a**, the main components were Fe, P, O, F, and C, consistent with the reaction system. To further verify the changes in elemental oxidation states and bond energies during the reaction, high-resolution Fe 2p, P 2p, C 1s and O 1s XPS spectra were obtained (**Figure S15b, c, d** and **e**). The Fe 2p spectrum of S-LFP involves two characteristic peaks at 711.5 eV and 726.8 eV for the Fe $2p_{3/2}$ and Fe $2p_{1/2}$ states, respectively. In detail, the Fe $2p_{3/2}$ peak and Fe $2p_{1/2}$ peaks can be deconvoluted into two peaks, correspond to the oxidation states Fe^{2+} (709.2 eV and 722.7 eV) and Fe^{3+} (711.3 eV and 725.5 eV), respectively. After regeneration, R-LFP also exhibited two characteristic peaks at 710.5 eV and 723.8 eV, which can be deconvoluted into Fe^{2+} peak and Fe^{3+} peak, consistent with the XPS spectra of S-LFP sample. The P 2p spectrum of S-LFP and R-LFP is not much different, which can be deconvoluted into two peaks (P $2p_{1/2}$ and P $2p_{3/2}$). C-F and C=C appear on the surface of S-LFP, indicating that the surface structure of S-LFP collapses and phase transition occurs. The surface of R-LFP is C=O and C-C, and the phase is relatively pure. Besides, the O 1s spectrum was deconvoluted into two peaks corresponding to two different kinds of bonds: the strong peak at 531.8 eV was related to P-O, and the weak peak at 532.5 eV can be ascribed to Fe-O moieties on the surface (**Figure S15e**).

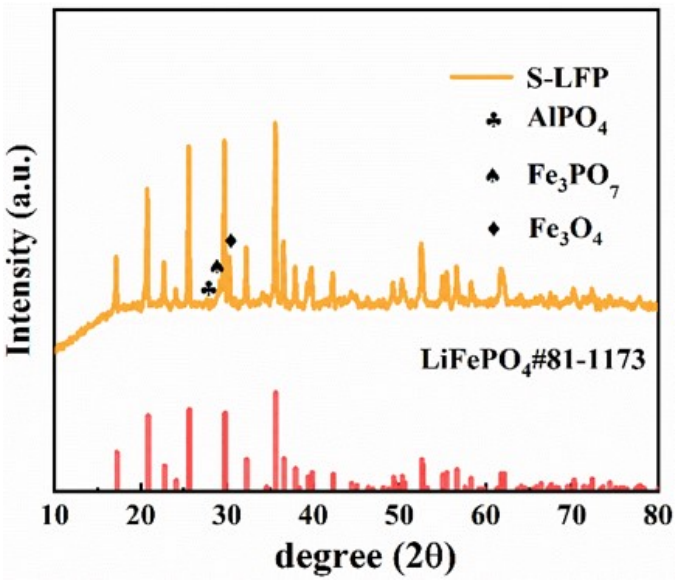

Figure S4 The XRD pattern of spent LFP cathode materials.

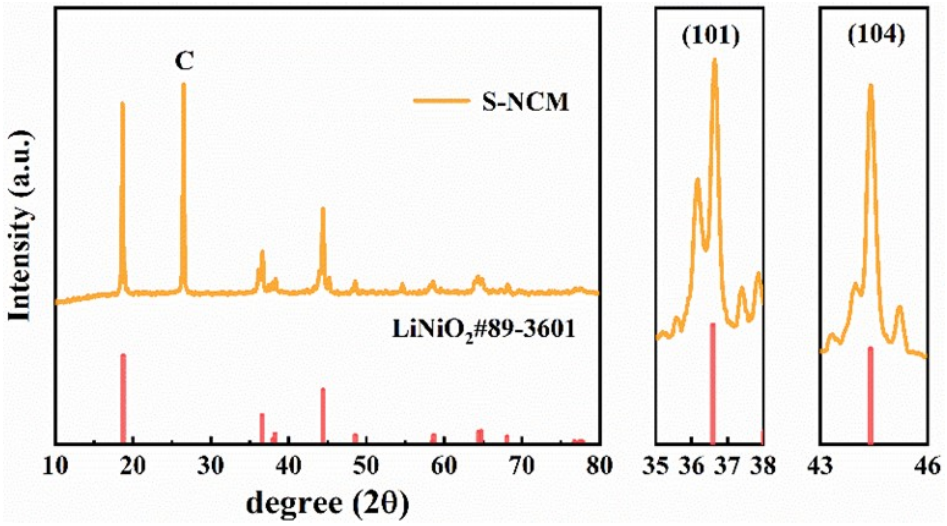

Figure S5 The XRD pattern of spent NCM cathode materials and magnification of (101) and (104) peaks.

The weak acid condition was first introduced to the LFP and NCM cathode materials individually to investigate the synergistic redox processes. Figure S6a demonstrates that weak acid has a good leaching effect on S-LFP, with Li, Fe, and P leaching rates exceeding 98%. In contrast, the leaching effect of S-NCM is notably different, with low leaching rates of Li, Ni, Co, and Mn *i.e.*, 75.83%, 35.58%, 33.17%, and 39.53%, respectively. The leaching of S-NCM without any additional agent is not ideal. The conventional approach is to add a reducing agent to enhance the leaching rate of Li, Ni, Co, and Mn, which will increase the cost.

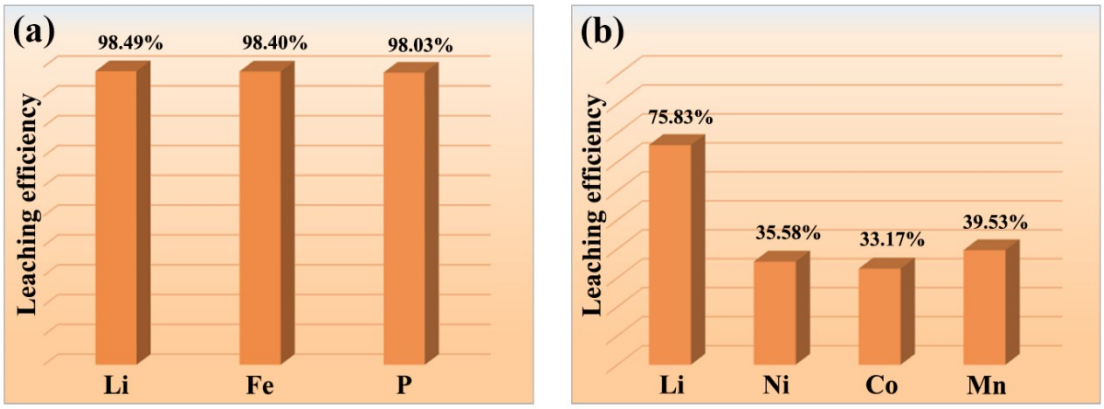

Figure S6. (a) Leaching efficiency of various elements of S-LFP by 3 mol/L sulfuric acid; (b) Leaching efficiency of various elements in 3 mol/L sulfuric acid leaching of S-NCM.

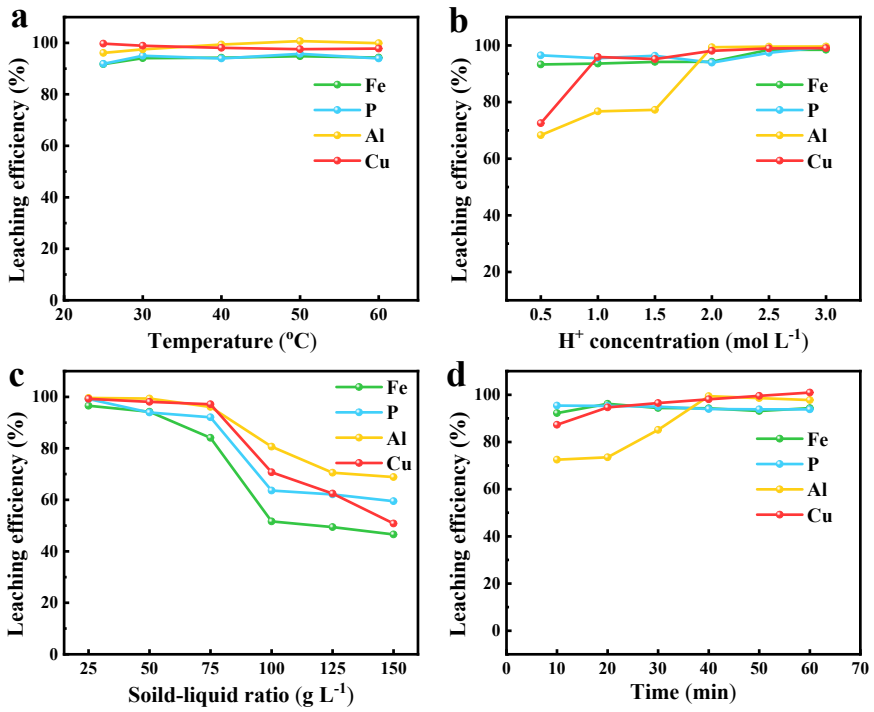

Figure S7 The effects on leaching efficiency for Fe, P, Al and Cu of (a) reaction temperature at 1 mol L^{-1} H^+ solution, S-L ratio of 50 g L^{-1} and 40 min; (b) H^+ concentration at 25 °C, S-L ratio of 50 g L^{-1} and 40 min; (c) solid-liquid ratio at 25 °C, 1 mol L^{-1} H^+ solution and 40 min; (d) leaching time at 30 min, 25 °C, 1 mol L^{-1} H^+ solution and S-L ratio of 50 g L^{-1}.

As shown in Figure. S8 and S9, the influence of mixing ratio on the leaching rate of each element was studied. It was found that when the mixing ratio was low, the leaching rate of Li, Ni, Co and Mn

was not high, because the lack of LFP, which could not produce enough Fe^{2+} and could not leach Li, Ni, Co and Mn in NCM into solution. With the increase of mixing ratio, the leaching rate of Li, Ni, Co and Mn gradually increased, when the mixing ratio was about 1.25, the leaching rate of Li, Ni, Co and Mn was close to 100%, and no longer increased. In this process, the leaching rate of Fe, P, Al and Cu is almost constant. Therefore, the optimal mixing ratio is 1.25.

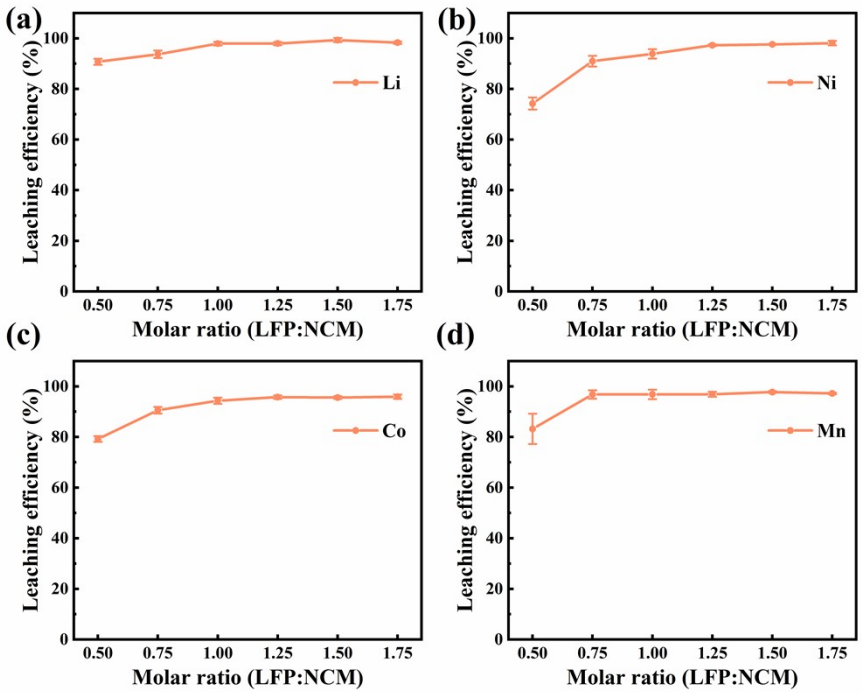

Figure S8 The effects on leaching efficiency for (a) Li, (b) Ni, (c) Co and (d) Mn of molar ratio (LFP:NCM)

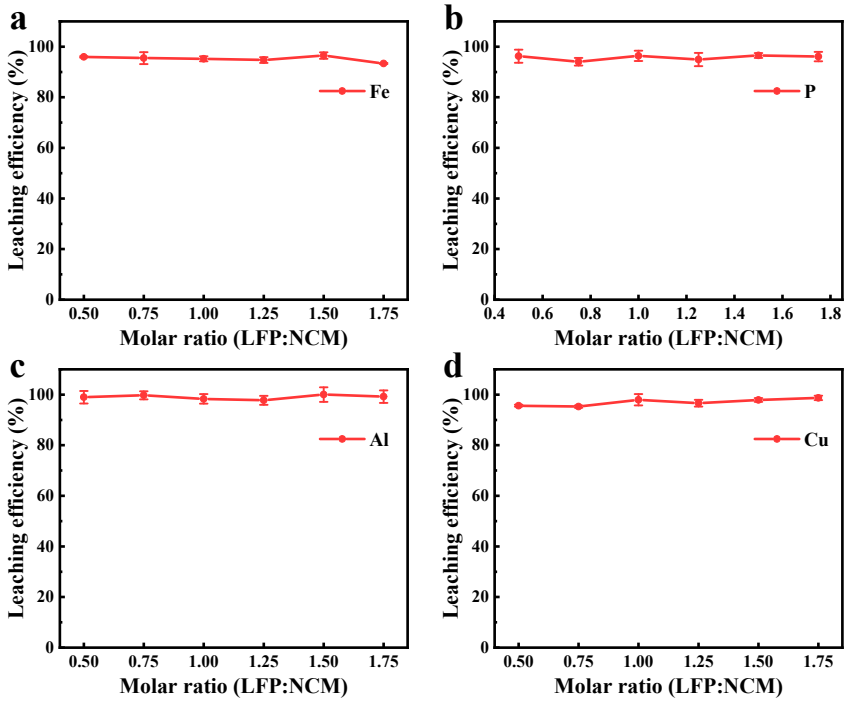

Figure S9 The effects on leaching efficiency for Fe, P, Al and Cu at different molar ratio between $LiFePO_4$ and $LiNi_xCo_yMn_{1-x-y}O_2$.

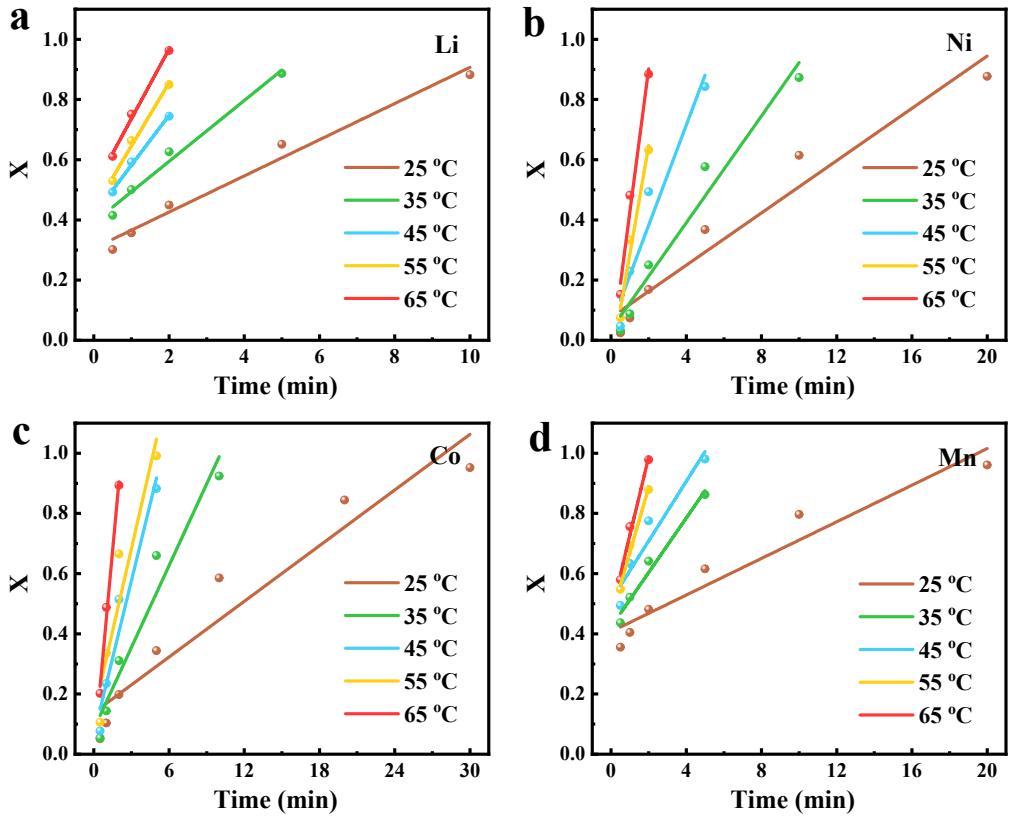

Figure S10 Data fitting diagram of external diffusion at different temperature and time for Li, Ni, Co and Mn.

Table S5 The value of R^2 (error sum of squares) for external diffusion kinetic mode.

Elements	25 °C	35 °C	45 °C	55 °C	65 °C
Li	0.98065	0.98458	0.99504	0.99096	0.99447
Ni	0.94954	0.96635	0.94044	0.9779	0.98231
Co	0.9267	0.9473	0.9511	0.8993	0.99186
Mn	0.93156	0.97423	0.9228	0.98609	0.98508

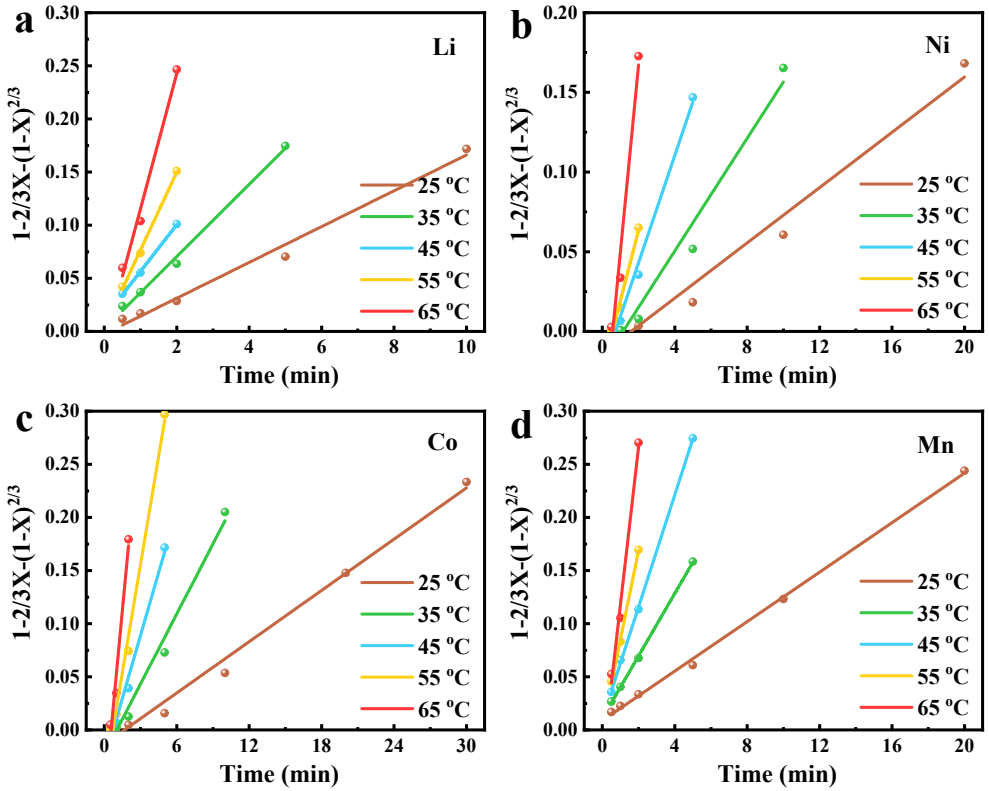

Figure S11 Data fitting diagram of internal diffusion at different temperature and time for Li, Ni, Co and Mn.

Table S6 The value of R^2 (error sum of squares) for internal diffusion kinetic mode.

Elements	25 °C	35 °C	45 °C	55 °C	65 °C
Li	0.98811	0.99498	0.99888	0.99789	0.98871
Ni	0.97814	0.97269	0.99057	0.98441	0.97404
Co	0.99046	0.98349	0.98762	0.99167	0.96995
Mn	0.99851	0.99942	0.99962	0.99867	0.9038

Table S7 The slope of the fitting curve for chemical reaction kinetic mode.

Elements	25 °C	35 °C	45 °C	55 °C	65 °C
Li	0.04147	0.07794	0.10828	0.16404	0.26812
Ni	0.02656	0.06783	0.18204	0.18204	0.31871
Co	0.02104	0.05886	0.17911	0.17911	0.30546
Mn	0.02526	0.05162	0.16966	0.16966	0.30706

Table S8 The value of apparent activation energy for Li, Ni, Co and Mn in references and this work.

Li (kJ mol^{-1})	Ni (kJ mol^{-1})	Co (kJ mol^{-1})	Mn (kJ mol^{-1})	Ref.
49.76	48.55	50.05	47.64	[1]
39.6	57.2	56.6	55.7	[2]
40.6	42.2	42.8	43.8	[3]
43.61	41.16	41.52	41.64	[4]
37.58	51.92	54.46	50.15	This work

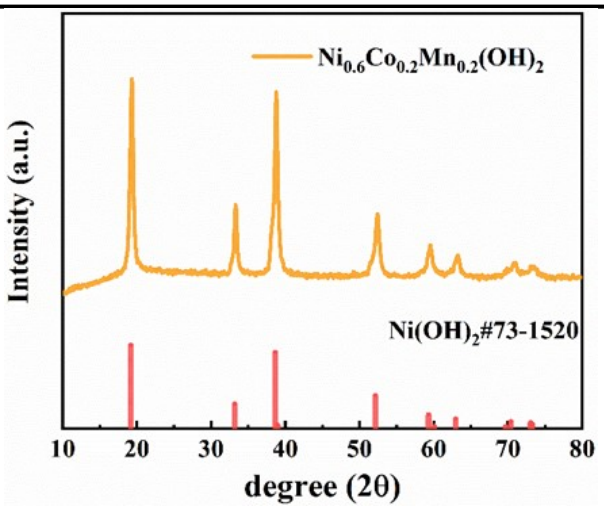

Figure S12 The XRD pattern of NCM (622) precursor materials.

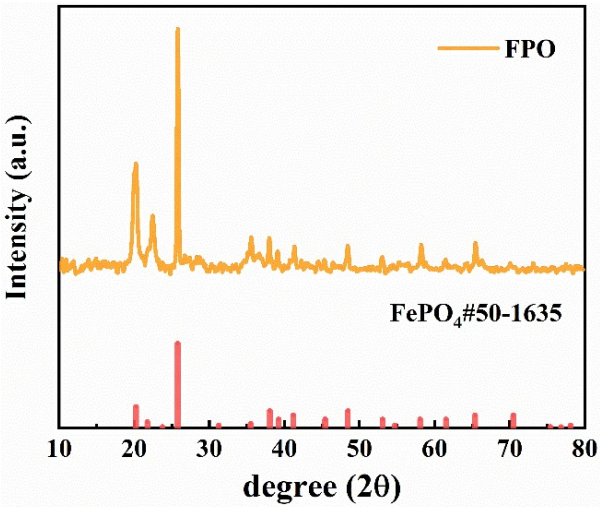

Figure S13 The XRD pattern of $FePO_4$ precursor materials.

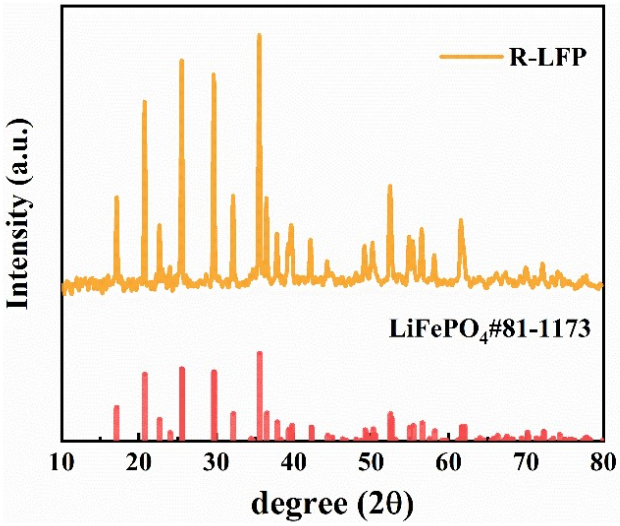

Figure S14 The XRD pattern of reprepared $LiFePO_4$ materials.

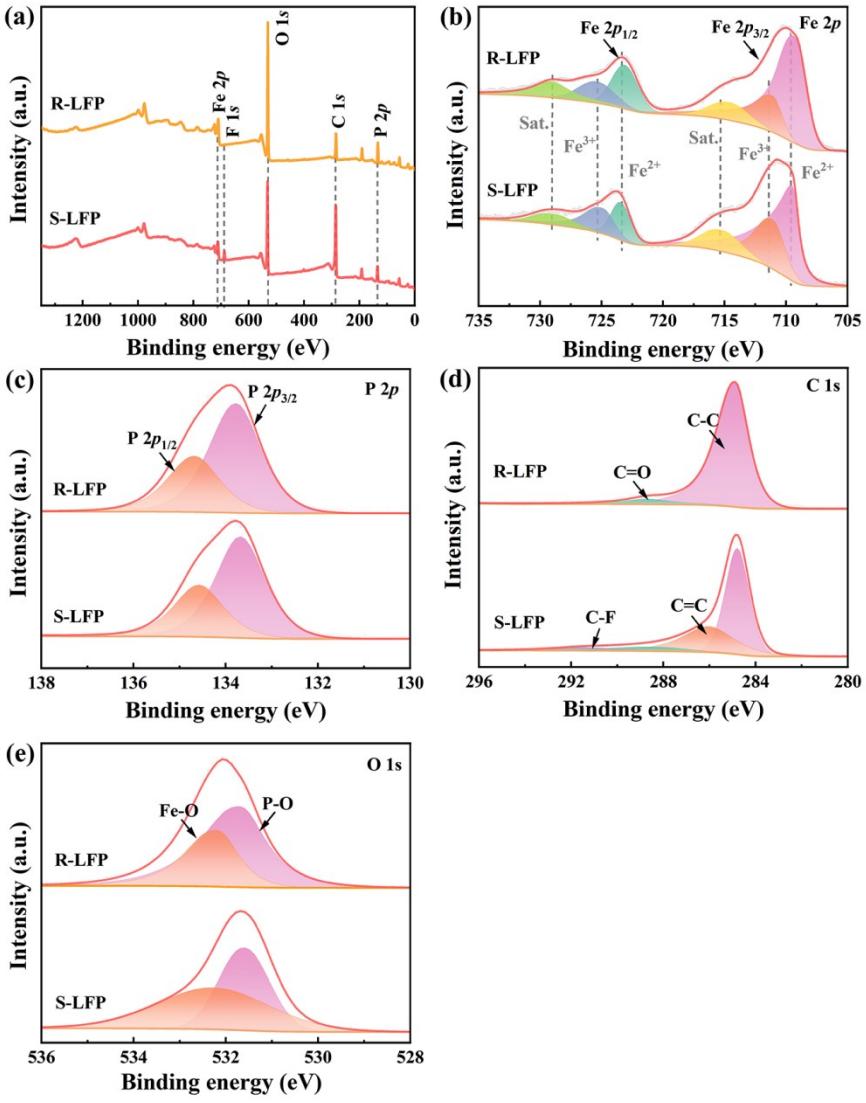

Figure S15 (a) XPS survey spectra of S-LFP and R-LFP, (b) Fe 2p XPS spectra of S-LFP and R-LFP, (c) P 2p XPS spectra of S-LFP and R-LFP, (d) C 1s XPS spectra of S-LFP and R-LFP, (e) O 1s XPS spectra of S-LFP and R-LFP.

Table S9 The price and quantity of raw materials

	Price(RMB)	**Quality**	**Data source**
Lithium iron phosphate battery	12000/t	0.678t	https://b2b.baidu.com/
Nickel-cobalt-manganate lithium battery	18000/t	0.322t	https://jiage.cngold.org/
Copper foil	67300/t	0.068*0.678+0.08*0.322=0.072t	https://jiage.cngold.org/
Aluminum foil	19150/t	0.052*0.678+0.07*0.322=0.0578t	https://www.zz91.com/
diaphragm	1500/t	0.0039*0.678+0.004*0.322=0.00393t	https://b2b.baidu.com/
graphite	8000/t	0.132*0.678+0.15*0.322=0.1378t	https://jiage.cngold.org/
Aluminium case	16450/t	0.136*0.678+0.14*0.322=0.1373t	
electrolyte	4500/t	0.098*0.678+0.10*0.322=0.0986t	
Sulfuric acid	1600/t	0.3105*1000000/50*0.5*98=0.3043t	http://www.100ppi.com/
Sodium carbonate	2650/t	（0.306*0.678/158+0.32*0.322/98）/2*1.4*106=0.1754t	http://soda.100ppi.com/
Ammonium bicarbonate	1950/t	0.32*0.322/98*2*1.4*84=0.2473t	http://www.100ppi.com/
20%Ammonia liquor	1600/t	0.3043/98*2*35=0.2174t	http://www.100ppi.com/
H2O	3.14/t	0.3105/50*1000=6.21t	https://www.h2o-china.com/
Lithium iron phosphate	160000/t	0.306*0.678*0.90=0.18675t	http://www.100ppi.com/
Lithium nickel-cobalt-manganate	416500/t	0.32*0.322*0.90=0.09274t	https://news.10jqka.com.cn/

glucose	4400/t	0.306*0.678*0.95*0.1=0.020t	http://chem.100ppi.com/

Table S10 Chemical reagents, energy consumption and pollution treatment

Chemical reagent consumption	leach	roast	Recover lithium	Precursor recovery	Positive electrode regeneration process	Total price	
	0.33955	0	0.05814	0	0.01985	0.41754	
	0	0.7694	0.16169	0	0	0.93109	
	1.38483	0	0.09443	1.59111	0	3.07037	
	0	0.11782	0.09484	0.3513	0	0.56396	
	0.05716	0	0.07232	0.12916	0.01369	0.27233	
Energy consumption	leach	roast	mix	desiccation	filtration	Total price	
	0.05856	0.17156	0.00441	0.01494	0.0244	0.27387	
	0.05856	0.444	0.00952	0.0075	0.01565	0.53523	
	0.12249	0.20742	0.00445	0.01506	0.07838	0.4278	
	0.19053	0.46284	0.02144	0.02144	0.07939	0.77564	
	0.06262	0.24947	0.00587	0.01989	0.03714	0.37499	
Pollution treatment	Waste water	Exhaust	Waste slag	Total price			
	0.09663	0.01556	7.78E-04	1.13E-01			
	0.10332	0.3112	0.1167	5.31E-01			
	1.22345	0.3112	7.78E-04	1.54E+00			
	0.6196	1.556	0.1167	2.29E+00			
	0.09663	7.78E-04	7.78E-04	9.82E-02			
Battery disassembly	Copper foil	Aluminu	diaphragm	graphite	Aluminium case	electrolyt	Total

	4576.4	995.8	5.85	1056	2237.2	441	9312.2
	4576.4	995.8	5.85	1056	2237.2	441	9312.2
	5384	1340.5	6	1200	2303	450	10683.
	5384	1340.5	6	1200	2303	450	10683.
	4845.6	1106.87	5.895	1102.4	2258.585	443.7	9763.0
	income/t						
The positive pole regenerates income	44064						
	36798.7						
	119952						
	119952						
	68506.21						

Table S11 Comprehensive economic calculation of various methods

	Recycled materials revenue	Battery disassembly accessories for profit	Chemical reagent consumption	Energy consumption	Pollution treatment	Equipment maintenance cost	Service charge	profit
Hy-LFP-Hy-NCM	10.65859004	1.517690113	1.27175126	0.32343546	5.71E-01	1.065859004	1.06585 9004	7.88E+00
Hy-LFP-Py-NCM	10.65859004	1.517690113	0.46468724	0.43543994	8.15E-01	1.065859004	1.06585 9004	8.33E+00
Py-LFP-Hy-NCM	9.892124141	1.517690113	1.61993816	0.50063754	8.55E-01	0.989212414	0.98921 2414	6.46E+00
Py-LFP-Py-LFP	9.892124141	1.517690113	0.81287414	0.61264202	1.10E+00	0.989212414	0.98921 2414	6.91E+00
This method	10.65956628	1.51913058	0.27233	0.37499	9.82E-02	1.065956628	1.06595 6628	9.30E+00

1. Chen, X.; Kang, D.; Li, J.; Zhou, T.; Ma, H., J. Hazard. Mater. 2019, 389, (5), 121887.
2. Xiao, X.; Hoogendoorn, B. W.; Ma, Y. Q.; Sahadevan, S. A.; Gardner, J. M.; Forsberg, K.; Olsson, R. T., Green Chem. 2021, 23, (21), 8519-8532.
3. Yan, S.; Sun, C.; Zhou, T.; Gao, R.; Xie, H., Sep. Purif. Technol. 2021, 257, 117930.
4. Gao, W.; Zhang, X.; Zheng, X.; Lin, X.; Cao, H.; Zhang, Y.; Sun, Z., Environ. Sci. Technol. 2017, 51, (3), 1662-1669.